nature climate change

Article

https://doi.org/10.1038/s41558-022-01555-7

Reduced CO_2 uptake and growing nutrient sequestration from slowing overturning circulation

In the format provided by the authors and unedited

Supplementary Information

Meridional Overturning Circulation in the CMIP5 and CMIP6 Models

There are substantial differences in the simulated global overturning circulation across the CMIP5 and CMIP6 models. The CMIP5 models have a larger spread (24 models) in the MOC rates compared to the CMIP6 models (Fig. 1, Extended Data Fig. 1, tables 1, S1). AMOC ranges widely from less than 5 Sv to 35 Sv from the preindustrial to the 2100s under the RCP8.5-ECP8.5 warming scenario, though almost all the models showed a decreasing trend as expected (Extended Data Fig. 1). Compared with the observational estimates, the strength of overturning circulation did not show noticeable improvement from CMIP5 to CMIP6. Both CMIP5 and CMIP6 models estimate the AMOC well at ~18Sv, consistent with observational estimates (table S1). However, both the CMIP5 and CMIP6 models strongly underestimate the strength of the SMOC (table S1). There are five models in CMIP5 extending to 2300, and all show continuing declines in the SMOC and the AMOC after year 2100 (Extended Data Fig. 1). CMIP6 model mean SMOC continues to decline to ~2 Sv by the year 2300. The model mean CMIP6 AMOC also has a large reduction before stabilizing at about 5 Sv (Fig. 1). Under moderate warming scenarios (SSP1-2.6 and SSP2-4.5), both AMOC and SMOC weaken from the preindustrial to 2100, but they decline more slowly than under SSP5-8.5 (Fig. 1, Extended Data Fig. 1).

Shutdown of AABW Formation and the SMOC in CESMv1

AABW formation slows due to increasing stratification in the Weddell Sea and the Ross Sea, key formation regions for AABW formation, which leads to the slowdown of the SMOC. The slowdown and apparent shutoff of dense AABW formation is noticeable in the oxygen fields averaged over the shelf depths (200-400m, Extended Data Fig. 2A). Early in the simulation, high oxygen concentrations are seen in the southern Weddell and Ross seas, indicating waters recently in contact with the atmosphere. Over time the increasing stratification breaks the connection to surface waters, and oxygen concentrations then approach the much lower values seen offshore, first in the Weddell Sea by the 2090s and with only a small patch of high O_2 water in the Ross Sea by the 2190s (Extended Data Fig. 2A). By the 2290s oxygen concentrations decline dramatically across the Southern Ocean at these depths as increasing temperatures, decrease density at the surface, and increasing stratification that ensures that winter mixing does not reach 200m depth in the region. The low oxygen concentrations demonstrate this lack of ventilation (Extended Data Fig. 2A).

Stratification in the Weddell Sea (< 60 ºS) increases rapidly beginning just before the year 2100 and levels out near the end of the simulation after rising by more than a factor of 2 (Extended Data Fig. 2B). The increase is more gradual in the Ross Sea and begins earlier, though the increase in both regions it accelerates with increasing loss of the southern sea ice cover (12). The increasing stratification in both regions is primarily driven by reductions in surface salinity. The southern Weddell and Ross seas do not warm as much with climate change (1-2°C) as the offshore waters of the Southern Ocean (~6-9 °C) by 2300. These regions are kept cooler by the cold winds blowing off Antarctica and are the only place in the Southern Ocean where some sea ice still forms by 2300 (12). The salinity-driven vertical density gradients in the high latitude Southern Ocean and a strongly salinity-dominated Arctic Ocean stratification suggest that polar ocean physics, circulation, and biogeochemistry will be sensitive to increasing freshwater runoff from the Greenland and Antarctic ice sheets with climate warming.

Factors Influencing the strength and volume of SMOC in the CMIP6 models

The strength of SMOC is defined as the maximum northward transport between 2500 and 5000m at the latitude 30°S, across the CMIP6 models that SMOC ranges widely, from 2 Sv to 15 Sv in the present climate. One important reason is that the surface buoyancy forcing is not well constrained, making it challenging to assess the fidelity of the AABW formation rate. Extended Data Fig. 2C shows the negative correlation between upper ocean stratification (density difference between 400m and 10m) in the latitudes 75°S-65°S and the strength of SMOC. The models with strong upper ocean stratification most underestimated SMOC, including CESMv2 and CIESM (models 5 and 9). The relative fraction of SMOC and AMOC to the global MOC is significant for circulation and ocean carbon storage patterns. The depth of the boundary between the MOC cells ranges widely in the CMIP6 models (Extended Data Fig. 2D). In the models with a deep separation boundary, the upper cell extends deeper, which squeezes the abyssal cell into a small depth band and decreases its northward transport.

Ocean Carbon Storage in the CMIP6 Models

We compared carbon sequestration in the CMIP6 models that reported the variables needed to compute the sequestration and in the CESMv1 out to year 2100. We use the AOU method to separate regenerated DIC from the preformed DIC for the CMIP6 models, which implies that the carbon regeneration due to $CaCO_3$ dissolution is lumped into the preformed DIC component. Thus, the preformed DIC is likely somewhat overestimated. All the models showed increasing storage of total DIC, regenerated DIC, and preformed DIC from the preindustrial era to 2100. In the deep ocean (> 2000m) the accumulation of regenerated DIC increases more quickly than preformed DIC storage, and accounts for 50% or more of deep ocean DIC storage by 2100 in all the models (Extended Data Figs. 3-5).

In terms of the models with remineralization outputs available (variable name "remoc"), we separated the regenerated DIC into both biological and circulation-driven fractions (Extended Data Fig. 8). The models consistently show a decreasing biological surface export of carbon in a warming climate. However, the increase in the regenerated DIC from the slowing circulation more than compensates (Extended Data Fig. 8). These results support our conclusion that most of the carbon accumulation in the deep ocean is due to the slowdown of global overturning circulation that dominates over the decreasing (or flat in a couple of models) export flux from the surface.

Ocean Carbon Storage in CESMv1 (RCP8.5-ECP8.5)

Global Ocean dissolved inorganic carbon concentrations gradually increase over time as the oceans take up more and more anthropogenic CO_2, especially in the Southern Ocean. Ocean uptake of CO_2 peaks at ~5.5 PgC/yr in the late 21st century and then declines steadily over time, even as atmospheric CO_2 continues to rise, as surface waters become increasingly saturated (12, 45). The DIC increase in the surface ocean is much larger than in the deep ocean, due to the direct uptake of anthropogenic CO_2 from the atmosphere (Extended Data Fig. 4). In the deep ocean, the DIC buildup over time is due mainly to the accumulation of carbon via the biological pump (~93% of deep ocean DIC increase). Thus, preformed DIC, which could include both natural and anthropogenic carbon, accounts for only ~7% of the deep ocean DIC storage by year 2300 (Extended Data Fig. 4).

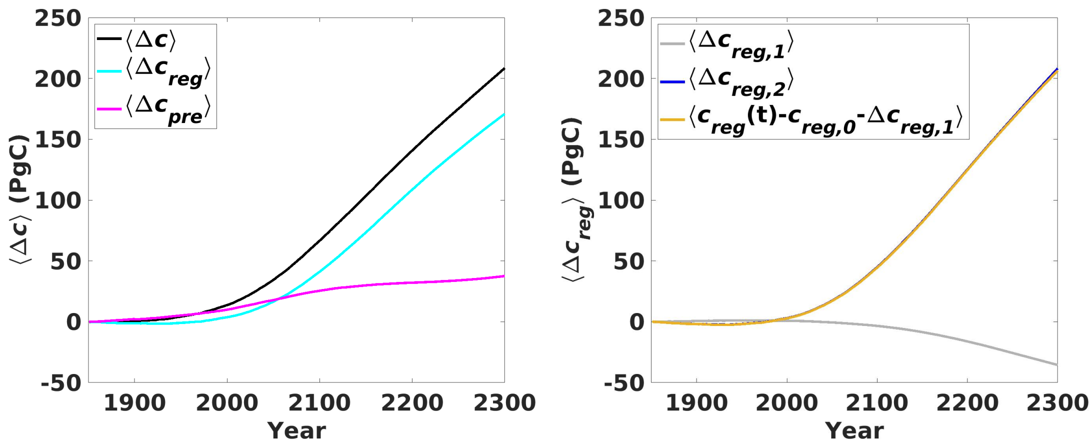

Supplementary Information Figure 1. Partitioning of deep-ocean DIC storage in the offline model. Left panel shows changes in the deep-ocean carbon inventory, $\langle \Delta c \rangle$, partitioned into preformed $\langle \Delta c_{pre} \rangle$ and regenerated $\langle \Delta c_{reg} \rangle$ parts. The right panel shows the changes in the deep-ocean (depth > 2000 m) regenerated carbon inventory separated into the part remineralized before 1850 (gray line), a part that is due to change in the post-1850 regeneration rate computed by fixing the transport operator to its 1850 value (dark yellow). The blue line is nearly identical to dark yellow line, indicating that equation (13) is a good approximation of equation (12), see Methods. The angle brackets denote the volume integral over depths greater than 2000 m.

	AOU method (Pg/yr)				TOU method (Pg/yr)				Offline model (Pg/yr)			
	1900s	2000s	2100s	2200s	1900s	2000s	2100s	2200s	1900s	2000s	2100s	2200s
0-100m	0.03	-0.00	-0.11	-0.12	0.02	-0.01	-0.11	-0.12	0.00	0.00	-0.00	-0.00
100-2000m	0.02	0.23	0.37	0.16	-0.00	0.22	0.28	0.04	0.06	0.21	0.15	-0.02
>2000m	0.04	0.29	0.51	0.60	0.03	0.32	0.61	0.73	0.04	0.33	0.62	0.56

Supplementary Information Figure 2. Comparison of the regenerated DIC accumulation calculated by the AOU method, TOU method and the offline model. The regenerated DIC accumulation rates in the surface ocean (0-100m), intermediate depths (100-2000m), and deep ocean (>2000m) averaged over the periods 1990-2000, 2000-2100, 2100-2200, and 2200-2300 computed from the AOU method in CESMv1 (left panel), TOU method (middle panel) and with the offline model (right panel) (PgC/yr).

Supplemental Tables

Supplementary Table S1. **The CMIP6 models included in the MOC analysis.** The 36 CMIP6 models included in the meridional overturning circulation computation. Only models with all necessary outputs available and a net northward bottom flow out of the Southern Ocean were included. Extended output to year 2300 was only available for a subset of the models. "Yes" indicates model output available and no indicates not available.

	Model name	Historical	SSP5-8.5		SSP2-4.5		SSP1-2.6	
			To 2100	To 2300	To 2100	To 2300	To 2100	To 2300
1	ACCESS-CM2	Yes	Yes	No	Yes	No	Yes	Yes
2	ACCESS-ESM1-5	Yes	Yes	No	Yes	No	Yes	Yes
3	BCC-CSM2-MR	Yes	Yes	No	Yes	No	Yes	No
4	CanESM5	Yes	Yes	Yes	Yes	No	Yes	Yes
5	CanESM5-CanOE	Yes	Yes	No	Yes	No	Yes	No
6	CESM2	Yes	Yes	No	Yes	No	Yes	No
7	CESM2-FV2	Yes	No	No	No	No	No	No
8	CESM2-WACCM	Yes	Yes	Yes	Yes	No	Yes	Yes
9	CESM2-WACCM-FV2	Yes	No	No	No	No	No	No
10	CIESM	Yes	Yes	No	Yes	No	Yes	No
11	CMCC-CM2-SR5	Yes	Yes	No	Yes	No	Yes	No
12	CMCC-ESM2	Yes	Yes	No	Yes	No	Yes	No
13	CNRM-ESM2-1	Yes	Yes	No	Yes	No	Yes	No
14	EC-Earth3	Yes	Yes	No	Yes	No	Yes	No
15	EC-Earth3-CC	Yes	Yes	No	Yes	No	No	No
16	EC-Earth3-Veg	Yes	Yes	No	Yes	No	Yes	No
17	FGOALS-f3-L	Yes	Yes	No	Yes	No	Yes	No
18	FGOALS-g3	Yes	Yes	No	Yes	No	Yes	No
19	GFDL-CM4	Yes	Yes	No	Yes	No	Yes	No
20	GFDL-ESM4	Yes	Yes	No	Yes	No	No	No
21	GISS-E2-1-G-CC	Yes	No	No	No	No	No	No
22	GISS-E2-1-G	Yes	No	No	No	No	No	No
23	INM-CM4-8	Yes	Yes	No	Yes	No	Yes	No
24	INM-CM5-0	Yes	Yes	No	Yes	No	Yes	No
25	IPSL-CM6A-LR	Yes	Yes	Yes	Yes	No	Yes	Yes
26	MIROC6	Yes	Yes	No	Yes	No	Yes	No
27	MIROC-ES2L	Yes	Yes	No	Yes	No	Yes	No
28	MPI-ESM1-2-HAM	Yes	No	No	No	No	No	No
29	MPI-ESM1-2-HR	Yes	Yes	No	Yes	No	Yes	No
30	MPI-ESM1-2-LR	Yes	Yes	No	Yes	No	Yes	No

31	MRI-ESM2-0	Yes	Yes	Yes	Yes	No	Yes	Yes
32	NorCPM1	Yes	No	No	No	No	No	No
33	NorESM2-LM	Yes	Yes	No	Yes	No	Yes	No
34	NorESM2-MM	Yes	Yes	No	No	No	No	No
35	SAM0-UNICON	Yes	No	No	No	No	No	No
36	UKESM1-0-LL	Yes	Yes	No	Yes	No	Yes	No

Supplementary Table S2. **The CMIP5 models included in the MOC analysis.** The 24 CMIP5 models included in the meridional overturning circulation computation under RCP8.5 warming scenario. Only the models with necessary outputs available and some net northward bottom flow out of the Southern Ocean were included. Extended output to year 2300 was only available for a subset of the models.

	Model name	Historical	To 2100	To 2300
1	ACCESS1-0	Yes	Yes	No
2	ACCESS1-3	Yes	Yes	No
3	CanESM2	Yes	Yes	No
4	CNRM-CM5	Yes	Yes	Yes
5	CSIRO-Mk3-6-0	Yes	Yes	Yes
6	FGOALS-g2	Yes	Yes	No
7	GFDL-CM3	Yes	Yes	No
8	GFDL-ESM2G	Yes	Yes	No
9	GFDL-ESM2M	Yes	Yes	No
10	GISS-E2-R	Yes	Yes	Yes
11	GISS-E2-R-CC	Yes	Yes	No
12	HadGEM2-CC	Yes	Yes	No
13	HadGEM2-ES	Yes	Yes	Yes
14	INMCM4	Yes	Yes	No
15	IPSL-CM5A-MR	Yes	Yes	No
16	IPSL-CM5A-LR	Yes	Yes	Yes
17	IPSL-CM5B-LR	Yes	Yes	No
18	MIROC5	Yes	Yes	No
19	MPI-ESM-MR	Yes	Yes	No
20	MPI-ESM-LR	Yes	Yes	No
21	MRI-CGCM3	Yes	Yes	No
22	MRI-ESM1	Yes	Yes	No
23	NorESM1-ME	Yes	Yes	No
24	NorESM1-M	Yes	Yes	No

Supplementary Table S3. **Model mean 1990s overturning rates from CMIP6 (36 models) and CMIP5 (24 models) for the Atlantic Meridional Overturning Circulation (AMOC) and the Southern Meridional Overturning Circulation (SMOC) cells are compared with observation-based estimates (reproduced from ref 28).** Maximum transport for AMOC is the maximum overturing at 30 ^{o}N over depths 0-3000 m. Maximum SMOC transport is the maximum overturning at 30^{o}S over the depth range 2500-5000 m.

	Estimate	Sources*	Transport at 30^{o}S (Sv)	Maximum transport (Sv)
			Models	
	CMIP5 Mean	1	12.0±4.7	17.1±5.8
	CMIP6 Mean	2	15.0±4.4	19.2±4.5
			Observation-based	
AMOC	Lumpkin & Speer, 2007 [54]	3	12	18
	Talley, 2013 [55]	3	13	18
	Meinen et al., 2018 [56]	4	15 (at 34.5^{o}S)	NA
	McCarthy et al., 2015 [57]	5	NA	17.0
	ECCO4	6	15	19
	Mean		13.8±1.5	18.0±0.8
			Transport at 30^{o}S (Sv)	
			Models	
	CMIP5 Mean	1	10.3±5.7	11.7±5.1
	CMIP6 Mean	2	6.7±3.4	8.4±3.5
			Observation-based	
SMOC	Talley, 2013 [55]	3	29	29
	Kunze, 2017 [58]	5	NA	20
	De Lavergne et al., 2016 [59]	5	NA	15
	Lumpkin & Speer, 2007 [54]	3	20.9	20.9
	ECCO4	6	15	20
	Mean		21.6±7.0	21.0±5.1

*: 1. CMIP5 model mean (24 models, Table S2); 2. CMIP6 model mean (36 models, Table S1); 3. Hydrography; 4. Moored density profiles; 5. Diapycnal mixing rates; 6. ECCO4, Estimating the Circulation and Climate of the Ocean v4 - assimilation of observations.